Check for updates
Natural Product Sciences
30(3) : 190-197 (2024)
https://doi.org/10.20307/nps.2024.30.3.190

Rutaecarpine, Isolated from *Evodia rutaecarpa*, Inhibits Epithelial-Mesenchymal Transition and Cellular Senescence in a Mouse Model of Pulmonary Fibrosis

Eun Choi[1], Yeseul Cho[1], Misu Kim[1], Hee Jin[1], Youngjo Yoo[1], Won Keun Oh[2,*], and Yun-sil Lee[1,*]

[1]*A Graduate School of Pharmaceutical Sciences, Ewha Womans University, Seoul 03760, Republic of Korea*
[2]*College of Pharmacy and Research Institute of Pharmaceutical Sciences, Seoul National University, Seoul 08826, Republic of Korea*

Abstract – Cellular senescence, a type of cytostasis, is the irreversible inhibition of the natural cell division in proliferating cells, resulting from various cellular stresses, including telomere shortening, DNA damage, mitochondrial dysfunctions, and pro-inflammatory responses. While cellular senescence can facilitate beneficial physiological processes such as tissue repair and wound healing, senescent cells also contribute to pathophysiological processes of age-related diseases, including fibrotic lung diseases. The cellular senescence model and co-culture system were established to explore the underlying mechanisms associated with cellular senescence and fibrosis. Rutaecarpine is a bioactive alkaloid isolated from *Evodia rutaecarpa* (Rutaceae), a traditional herbal medicine. Rutaecarpine enhanced the promotor activity of E-cadherin, reduced TGF-β-induced reorganization of the actin cytoskeleton, and finally inhibited epithelial-mesenchymal transition. Rutaecarpine also attenuated fibrotic and senescence features in bleomycin-induced lung fibrosis model. Here, we suggest the relevance between senescence and fibrosis, and a potential therapeutic approach of targeting senescence to attenuate lung fibrosis development.

Keywords – Pulmonary fibrosis, Rutaecarpine, Cellular senescence, Epithelial-mesenchymal transition

Introduction

Idiopathic pulmonary fibrosis (IPF) is a chronic and progressive lung disease with a poor prognosis, for which the exact cause is unknown. Epidemiological studies of IPF have revealed that the worldwide incidence and prevalence range between 0.09 and 1.30 per 10,000 individuals, growing every year. Among the countries investigated, the United States, South Korea, and Canada have the highest incidence rates.[1,2] Researchers have observed that IPF is characterized by an excessive buildup of the extracellular matrix (ECM) in the lungs, which distorts the normal lung structure and causes an irreversible loss of lung function.[3] IPF is a severe and chronic respiratory condition that leads to the formation of scar tissue in the lungs, gradually impairing breathing. There is a growing demand for more diverse therapeutic options for the treatment of IPF. To date, only two medications, nintedanib and pirfenidone (PFD), have received approval for treating patients diagnosed with IPF. Nintedanib is a tyrosine kinase inhibitor, while PFD exhibits antioxidant, anti-inflammatory, and anti-fibrotic effects. However, they have also been associated with some side effects and tolerability concerns.[4] Therefore, keeping up with recent advancements in IPF pathogenesis holds promise for the discovery of novel strategies to combat this devastating fibrotic lung disease.

Epithelial to mesenchymal transition (EMT) is a cellular process where epithelial cells endure a downregulation of their epithelial features and gain mesenchymal phenotypes and behavior. The regulation of EMT occurs through various factors, including transcriptional control, cell signaling, epigenetic modifications, and post-translational modifications. Cytokines such as TGF-β, fibroblast growth factors (FGFs), epidermal growth factor (EGF), and hepatocyte growth factor (HGF) are examples of signals that can induce or promote the EMT process. These EMT-inducing signals upregulate specific transcription factors known as EMT-TFs, including SNAI, TWIST, and ZEB.[5–8] In its initial stages, EMT occurs in cells that have apical-basal polarity, stable epithelial cell-cell junctions, and interactions with the basement membrane, representing an epithelial state. During EMT, alterations in gene

*Author for correspondence
Yun-Sil Lee, Ph.D, College of Pharmacy, Ewha Womans University, Seoul 03760, Republic of Korea
Tel: +82-02-3277-3022; E-mail: yslee0425@ewha.ac.kr
Won-Keun Oh, Ph.D, College of Pharmacy, Seoul National University, Seoul 08826, Republic of Korea
Tel: +82-2-880-7872; E-mail: wkoh1@snu.ac.kr

expression and post-translational regulatory mechanisms occur, resulting in the suppression of epithelial characteristics and the acquisition of mesenchymal traits.

The accumulation of fibroblasts in the pulmonary interstitium and the subsequent production of ECM are key processes in IPF.[9] Primary lung fibroblasts isolated from the lung tissue of IPF patients display a higher degree of senescence compared to age-matched controls. These senescent fibroblasts exhibit increased levels of SA-β-Gal (senescence-associated beta-galactosidase), p16, p21, p53, and SASP (senescence-associated secretory phenotype).[10] Targeting senescent fibroblasts and myofibroblasts using senolytic drugs has shown significant improvements in pulmonary fibrosis and function in mouse models of IPF.[11,12]

Evodiae Fructus, also known as Wu Zhu Yu, refers to the dried fruit of the shrubs or small trees belonging to the Rutaceae family, specifically *Evodia rutaecarpa* (Juss.) Benth. It has a long history of clinical use and is officially recognized in the Chinese Pharmacopeia 2015 Edition. Evodia Fructus is considered a geo-authentic crude drug with significant clinical efficacy.[13] The major bioactive compounds found in Evodia Fructus are alkaloids, including rutaecarpine (RUT), evodiamine (EVO), and dehydroevodiamine (DHED).[14] Extensive research has revealed various pharmacological actions of these alkaloids, such as anti-oxidant, vasodilatory, anti-cancer, anti-inflammatory, anti-fibrotic, anti-obesity, anti-platelet activation, and lipid-lowering effects. RUT, in particular, is one of the most notable indolopyridoquinazoline alkaloids derived from the fruit of *Evodia rutaecarpa* and has shown broad pharmacological benefits in treating cerebrovascular, cardiovascular, and metabolic diseases.[15] Few studies have reported the anti-fibrotic effect of RUT in pulmonary fibrosis models. In 2018, Gao et al. reported that RUT exhibited a protective effect against bleomycin (BLM)-induced pulmonary fibrosis by inhibiting Notch1/eIF3a signaling pathway. This inhibition led to the alleviation of the EMT process and increased synthesis and release of CGRP (Calcitonin gene-related peptide).[16] A recent study also reported that RUT ameliorated lipopolysaccharide-induced BEAS-2B cell injury through inhibition of ER (endoplasmic reticulum) stress via activation of the AMPK/SIRT1 (AMP-activated protein kinase/NAD-dependent deacetylase sirtuin-1) signaling pathway.[17]

In this study, we investigated the association between cellular senescence and the pathogenesis of fibrosis. Therapeutic strategy of enhancing E-cadherin level and alleviating activated fibroblasts-induced epithelial senescence may provide a potential novel therapeutic approach for IPF patients.

Experimental

Cell culture and transfection – The human embryo normal lung fibroblast cell line (IMR90) was cultured in Dulbecco's Modified Eagles Medium (DMEM) (#SH30243, HyClone, Logan, UT, USA) supplemented with 15% fetal bovine serum (Gibco, Waltham, MA, USA), 1% Penicillin Streptomycin Solution (100X, #CA005-010, GeneDEPOT, Katy, TX, USA) and 1% MEM Non-essential Amino Acid Solution (100x, #LS005-01, Welgene, Korea). Fibroblasts are classified as early-passage (under 20 passages), middle-passage (between 22 and 26 passages), and over-passaged (passages over 28). L132 cell line and HEK293T cell line were cultured in RPMI-1640 medium (Gibco) and Dulbecco's Minimal Essential Medium (DMEM) (Welgene), respectively, supplemented with 10% FBS and 1% penicillin at 37°C in a 5% CO_2 humidified incubator.

Compounds and chemicals – A library of natural products was kindly provided by Professor WK Oh (Seoul National University, Korea). RUT was purchased from Sigma-Aldrich (#R3277, St. Louis, MO, USA) after the screening. Pirfenidone (PFD) was purchased from TCI (#P1871, Tokyo Chemical Industry, Tokyo, Japan) as a positive control.

E-cadherin promoter assay – E-cadherin promoter activity was measured using a luciferase assay system kit (#E4030, Promega, Madison, WI, USA) in accordance with the manufacturer's instructions. The relative fluorescent unit (RFU) values were analyzed using the Infinite F200 PRO microplate multi-reader (Tecan, Männedorf Switzerland, equipped at Ewha Drug Development Research Core Center).

β-galactosidase staining – Cells were rinsed with 1X PBS and fixed with 1X fixative solution provided by the senescence β-galactosidase staining kit (#9860, Cell Signaling Technologies (CST), Beverly, MA, USA). Fresh β-galactosidase staining solution was prepared according to manufacturer's instructions. Cells in each dish were stained with 1mL staining solution after being washed with 1X PBS for 2 times. The staining process was accomplished after incubation at 37°C in a dry CO_2 incubator for 16–20 hours. The β-galactosidase positive cells were considered as senescent cells

Phalloidin staining – Morphological changes were investigated by Alexa 488-conjugated phalloidin staining (#A12379, Invitrogen, Carlsbad, CA, USA). Images were obtained using a Zeiss microscope Apotome (Cal Zeiss, Oberkochen, Germany, equipped at Ewha Drug Development Research Core Center).

Western blotting – Antibodies used for immunoblotting

were as follows: anti-β-actin (#sc-47778), anti-p21 (#sc-6246), and anti-N-cadherin (#sc-59987), were purchased from Santa Cruz biotechnology (SCB, CA, USA); anti-p16 (#80772S), anti-Snail (#3895S), and anti-Slug (#9585S) were purchased from CST. Anti-E-cadherin (#610181) was purchased form BD Bioscience (Mountain View, CA); anti-α-SMA (#A5228, Sigma-Aldrich) was also used.

RNA isolation and quantitative reverse transcription polymerase chain reaction (qRT-PCR) – Total RNA was isolated from the sample using QIAzol® reagent (#79306, Qiazen, Valencia, CA, USA). RNA purity and concentration were measured with a Nanodrop (Thermo, MA, USA, equipped at Ewha Drug Development Research Core Center). RNA was reverse transcribed using a ReverTra Ace® qPCR RT Kit (#FSQ-101, TOYOBO, kita-ku, Osaka, Japan) following the manufacturer's protocol. The mRNA expression levels of CDH1 (E-cadherin), ZEB1, SNAI1, SNAI2 (SLUG), TWIST, and GAPDH were measured by quantitative real-time PCR using SensiFAST sybr Hi-Rox Mix (#Bio-92020, Bioline USA Inc, Taunton, MA, USA) with CFX96 Touch™ Real-Time PCR Detection System (Bio-Rad, Hercules, CA, USA). The $2^{-\Delta\Delta Ct}$ method was used to analyze the relative changes in gene expression based on real-time quantitative PCR. GAPDH was used as an internal control gene. Primer sequences for qRT-PCR are listed in Table 1.

Co-culture system – An indirect co-culture system was established by using cell culture inserts (0.4 μm PET, 4.5 cm^2, #036006, SPL life Sciences, Pyeongtaek, Korea). IMR-90 cells were pre-treated with or without 5 ng/mL TGF-β (#240-B, R&D systems, Minneapolis, MN, USA). In the co-culture system, IMR-90 cells were plated in the upper chamber with wash-off of TGF-β and L132 cells in the lower chamber. The cells were then co-cultured for another 3 days. After co-culturing, the inserts were removed, and L132 cells were harvested for further analysis.

Irradiation – Cells were plated in 35- or 60-mm dishes in medium and incubated at 37°C in a humidified 5% CO_2 atmosphere. The day after seeding, the cells were exposed to γ-ray using a ^{137}Cs γ-ray source (Elan 3000, Atomic Energy of Canada, Ontario, Canada) with a dose rate 2.23 Gy/min. All the cells irradiated with γ-rays in the experiment were treated with 10 Gy.

Animal experiments – Male C57BL/6 mice (age, 6 weeks; weight, 20–25 g) were purchased from Orient Bio (Seongnam, South Korea). All protocols involving the use of mice were approved by the Animal Care and Use Committees of Ewha Womans University and were performed in accordance with relevant guidelines. Mice were injected with BLM (2.5 mg/kg, #sc-200134, SCB) through the intratracheal route. The mice were intraperitoneally treated with RUT (2 mg/kg) every other day. Lung tissues were collected for further analysis. A single dose of 75 Gy radiation (IR) was delivered using an X-RAD 320 platform (Precision X-Ray, North Branford, CT) as described previously.[18] Lung tissues were collected at each time point after IR.

Histological and immunohistochemical analysis – Lung tissues were formalin-fixed, paraffin-embedded, and 4 μm tissue sections were prepared for Masson's trichrome (#HT-15, Sigma-Aldrich) collagen staining. Immunohistochemical (IHC) staining was carried out using anti-p16 (#80772s, CST), anti-β-Gal (#sc-377257, SCB), and E-cadherin (#610181, BD). Slides were then incubated with avidin-biotin-peroxidase complex (ABC kit, Vector Laboratories, CA, USA) and developed using 3,3′-diaminobenzidine tetrachloride (DAB; Zymed Laboratories, CA, USA). Quantification of positive staining was analyzed with ImageJ software using standard algorithms to define the areas of staining (ImageJ, National Institutes of Health, Bethesda).

Immunofluorescence staining – For lung tissue immunofluorescence staining, the sections were deparaffinized with xylene, dehydrated with ethanol, and then heated in 0.1 M citrate buffer (pH 6.0). Co-immunostaining with anti-p16 (#80772s, CST), anti E-cadherin (#610181, BD) and α-SMA (#A5228, Sigma-Aldrich) was conducted overnight at 4°C. Secondary antibodies were incubated at room temperature for 1 h. The nucleus was counterstained with 4′,6-diamino-2-phenylindole (DAPI; #F6057, Sigma-Aldrich). Images were viewed under a Zeiss Apotome microscope (Carl Zeiss).

Statistical analysis – Statistical significance was determined by ANOVA or Student's *t*-test. Differences were considered significant if the p value was < 0.05. Results are presented as means and standard deviation (SD) or standard error of the mean (SEM).

Results and Discussion

To first investigate whether senescence associated genes are altered in common fibroblast mouse models, microarray and RNA sequencing (RNA-seq) datasets of the BLM-induced fibrosis model and the 75 Gy focal irradiated fibrosis model were collected from our previous studies.[19] Relative expression levels of established senescence genes were analyzed compared to respective control groups. Microarray data revealed that senescence-associated genes such as *Cdkn1a* (p21) and *Cdkn2a*

(p16) were upregulated in both models, indicating a close association between aging and fibrosis (data not shown). To establish an IR-induced senescence model *in vitro*, SA-β-Gal staining was performed. Exposure of human WI-38 fibroblast to 5 Gy and 10 Gy irradiation induced a dose-dependent phenotype of cellular senescence observable after 9 days, which was confirmed by staining for SA-β-Gal (Fig. S1A). To identify aging- associated effects on fibrotic features, early passage cells (passage < 20), middle passage cells (passage 22 ~ 26) and over-passaged cells (passage > 27), which seem to reach complete cellular senescence, were compared. Aged cells demonstrated elevated senescence-associated markers (p16 and p21) with increased SA-β-Gal staining (Fig. S1B).

To establish a more defined *in vitro* model to understand the underlying mechanisms associated with cellular senescence and fibrosis, TGF-β, a key regulator of both cellular senescence and fibrosis, was treated as a trigger. To further confirm whether the pro-fibrotic role of senescent epithelial cells in IPF was induced by the activation of pulmonary fibroblasts, TGF-β pre-treated human pulmonary fibroblast IMR-90 cells were co-cultured with L132 cells, pulmonary epithelial cells. L132 cells were either directly treated with TGF-β or co-cultured with fibroblast with or without TGF-β pre-treatment. TGF-β containing media was removed and changed with fresh media to minimize the direct effect of TGF-β but limit the impact of activated fibroblasts on epithelial cell senescence (Fig. S1C). Morphological changes significantly reflected alterations in cellular processes. These processes may include cellular senescence and EMT. L132 cells exhibited significant morphological changes after the treatment with TGF-β. However, L132 cells co-cultured with fibroblasts or activated fibroblasts demonstrated a significant increase in enlarged, flattened and irregular shapes, more closely representing a senescent cell phenotype (Fig. S1D). To further understand the molecular changes engaged with these morphological changes, L132 cells were collected for further analysis. The epithelial marker, E-cadherin, was decreased by all three stimuli (direct TGF-β stimulus, stimulus by co-cultured fibroblasts, and stimulus by co-cultured activated fibroblasts). However, L132 cells co-cultured with non-activated fibroblasts showed only moderate alterations in the levels of E-cadherin and N-cadherin. L132 cells co-cultured with activated fibroblasts showed significant alterations in the levels of both E-cadherin and N-cadherin, similar to the extent of those in L132 cells directly activated with TGF-β. Transcription factors of E-cadherin (Snail and Slug) and senescence marker p16 showed similar changes. However, another senescence marker, p21, showed more significant elevation in co-cultured cells, with activated fibroblasts inducing an earlier elevation of p21 (Fig. S1E).

A natural compound library at a concentration of 10 μg/mL was screened for the promoter activity of E-cadherin. Positive candidates (52, 91, 153, and 248) and one negative candidate (607) were identified. PFD (2 μM), an FDA-approved anti-fibrosis drug, was used as a positive control (Fig. 1A). Compound 248 showed a dose-dependent increase in promoter activity of E-cadherin (Fig. 1B). 248 is known as RUT a bioactive alkaloid isolated from the fruit of *Evodia rutaecarpa* (Fig. 1C). TGF-β repressed E-cadherin expression at the mRNA level, but RUT treatment restored the mRNA level of E-cadherin (Fig. 1D). RUT also alleviated TGF-β-induced reorganization of the actin cytoskeleton in a dose-dependent manner (Fig. 1E). Transcription factors (TFs), such as Snail and Slug (also known as SNAI1 and SNAI2), control the down-regulation of E-cadherin by directly binding onto the conserved E-boxes (CANNTG sequences) in the E-cadherin promoter. RUT repressed all TFs, but statistical significance was only obtained with ZEB1 and Twist (Fig. 1F).

The anti-fibrotic effect of RUT was further validated in the BLM-induced fibrosis mouse model (Fig. 2A). Intraperitoneal injection of 2 mg/kg RUT every other day significantly ameliorated BLM-induced collagen deposition. RUT also reduced the BLM-induced increase of senescence-associated markers such as β-galactosidase and p16 (Fig. 2B). To further investigate whether the inhibition of epithelial cell senescence induced by activated fibroblasts could alleviate the pathogenesis of fibrosis, RUT was added into the culture medium of L132 cells. RUT treatment could enhance the expression of E-cadherin and inhibit the expression of N-cadherin in L132 cells co-cultured with activated fibroblasts. In addition, the expression of p16 was significantly down-regulated by the treatment of RUT (Fig. 2C).

Interestingly, E-cadherin level was exceptionally up-regulated in the 75 Gy radiation-induced lung fibrosis model and it could be explained as the number of senescent epithelial cells increases (Fig. 3A). Immunofluorescence staining demonstrated that epithelial cells expressing E-cadherin also showed p16 in its nucleus (Fig. 3B). To explore the potential involvement of epithelial senescence in pulmonary fibrosis, we analyzed the distribution of cell populations expressing the senescence marker CDKN2A (p16) and the epithelial marker CDH1 (E-cadherin) using single cell RNA-sequencing (scRNA-seq) data reported by Habermann et al.[20] Consistent with the immunofluorescence staining results, we identified a population of cells co-expressing CDH1 and CDKN2A, which

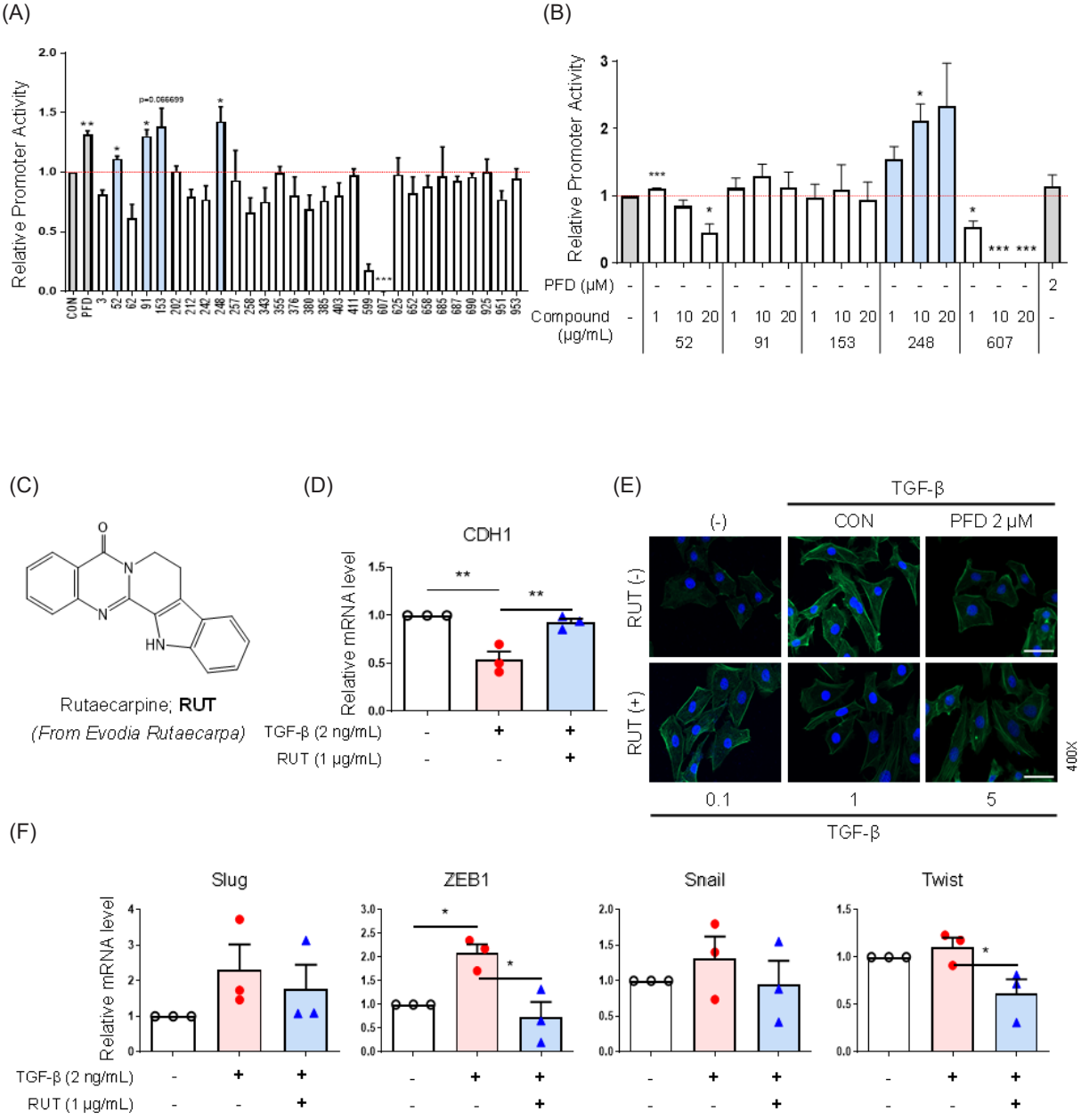

Fig. 1. Rutaecarpin alleviated E-cadherin expression and TGF-β-induced reorganization of actin cytoskeleton (A) L132 cells were transfected with pGL3 luciferase reporter vector containing the E-cadherin promoter, followed by 12 h of stimulation with a natural compound library (10 μg/mL) solubilized in DMSO. (B) Relative E-cadherin promoter activity of RUT dose-dependent changes. L132 cells were transfected with pGL3 luciferase reporter vector containing the E-cadherin promoter, followed by stimulation with different concentration of selected compounds solubilized in DMSO for 12 h. PFD was used as a positive control for E-cadherin promoter activity with 2 μM. The same volume of DMSO was added to the cells as controls. For each compound, the fold change in luciferase activity of stimulated cells was calculated relative to that of the DMSO control. Quantitative data are shown as mean ± SEM (n = 3/group), ***p < 0.001, **p < 0.01, *p < 0.05 vs. untreated control, Student's t-test. (C) A structure of RUT. (D) Relative mRNA level of E-cadherin after 24 h of TGF-β (2 ng/mL) treatment, with or without RUT (1 μg/mL) pre-treatment, using qRT-PCR in L132 cells. (E) Representative immunofluorescence image of actin skeleton reorganization (phalloidin; green) under TGF-β (10 ng/mL) stimuli. PFD at 2 μM was used as a positive control. Magnification, 400×. Scale bar, 50 μm. (F) Relative mRNA level of EMT-TFs (Slug, ZEB1, Snail, and Twist) using qRT-PCR in L132 cells. Cell lysates were collected Slug, ZEB1 after 6 h and Snail, Twist after 12 h of TGF-β (2 ng/mL) treatment, with or without RUT (1 μg/mL) pre-treatment. GAPDH mRNA was used for normalization. Subsequent statistical analysis was performed with one-way ANOVA with Bonferroni test for multiple comparisons **p < 0.01, *p < 0.05 vs. corresponding control.

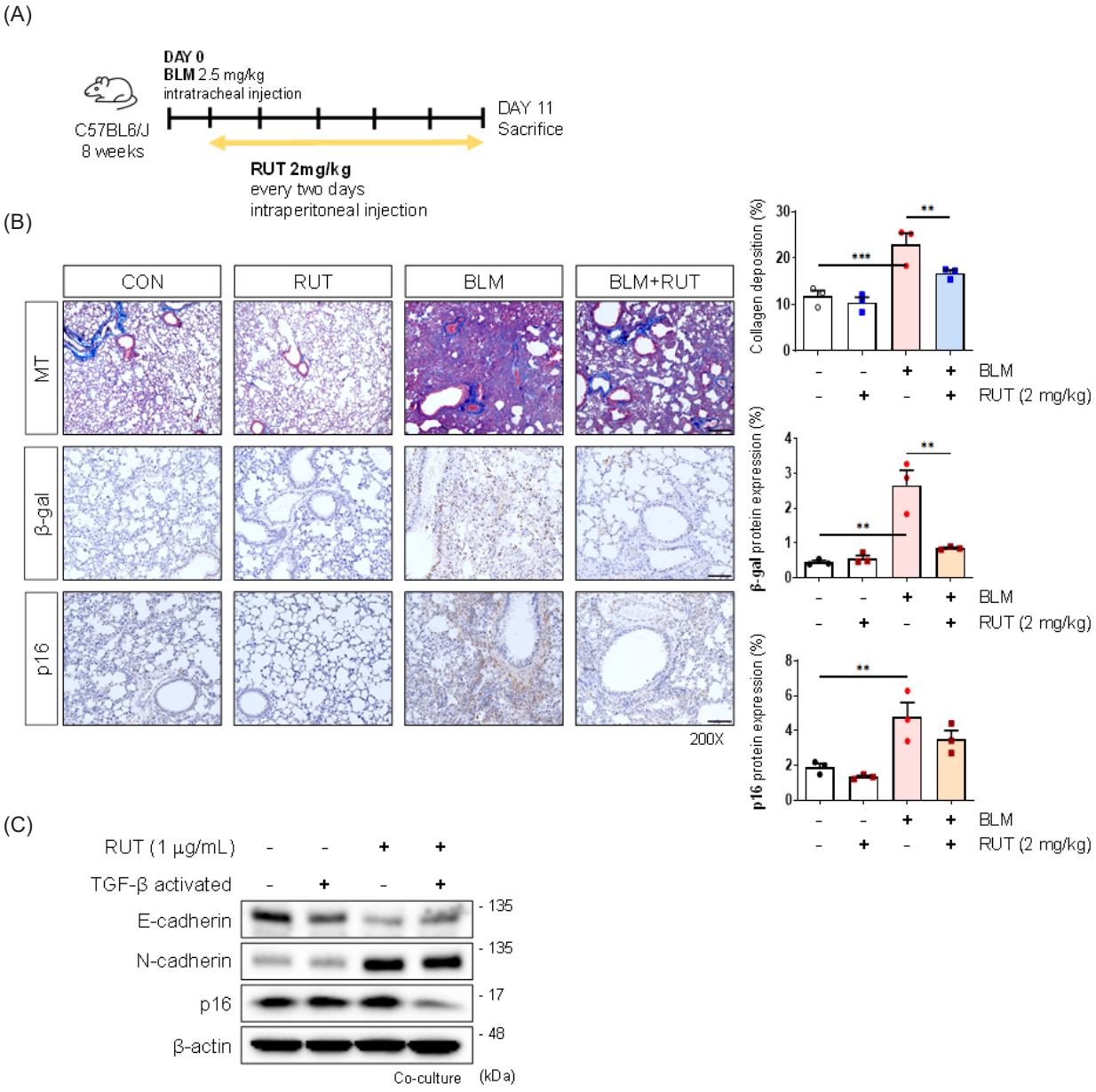

Fig. 2. Rutaecarpine attenuated both fibrosis and senescence associated markers in BLM-induced fibrosis model and co-culture system (A) Experimental scheme of BLM-induced PF mice model. (B) Histopathological analysis of lungs at indicated time points and quantification of each staining. (MT; mason-trichrome. SA-β-Gal; IHC staining of β-galactosidase. p16; IHC staining of p16) Magnification, 200×. Scale bar, 100 μm. (C) Western blot analysis using cell lysates 72 h after TGF-β (5 ng/mL) with or without RUT (1 μg/mL) pre-treatment in co-cultured activated fibroblasts. Subsequent statistical analysis was performed with unpaired one-way ANOVA with Bonferroni test for multiple comparisons ***$p < 0.001$, **$p < 0.01$.

was exclusively present in the epithelial cell population of IPF lung tissue (Fig. S2), suggesting the possibility of epithelial cells undergoing senescence in pulmonary fibrosis. E-cadherin level was exceptionally up-regulated in BLM model and it could be explained as the number of senescent epithelial cells increases. RUT alone increased the level of E-cadherin in mice model, but reduced the BLM-induced increase of E-cadherin (Fig. 3C), suggesting that RUT alleviated fibrosis through abolishing epithelial cell senescence. These results may refer to the close relationship between pulmonary fibrosis and cellular senescence and RUT, an enhancer of E-cadherin, may contribute to a potential therapeutic strategy of targeting senescence in pulmonary fibrosis.

Pulmonary fibrosis involves a process called EMT, in which

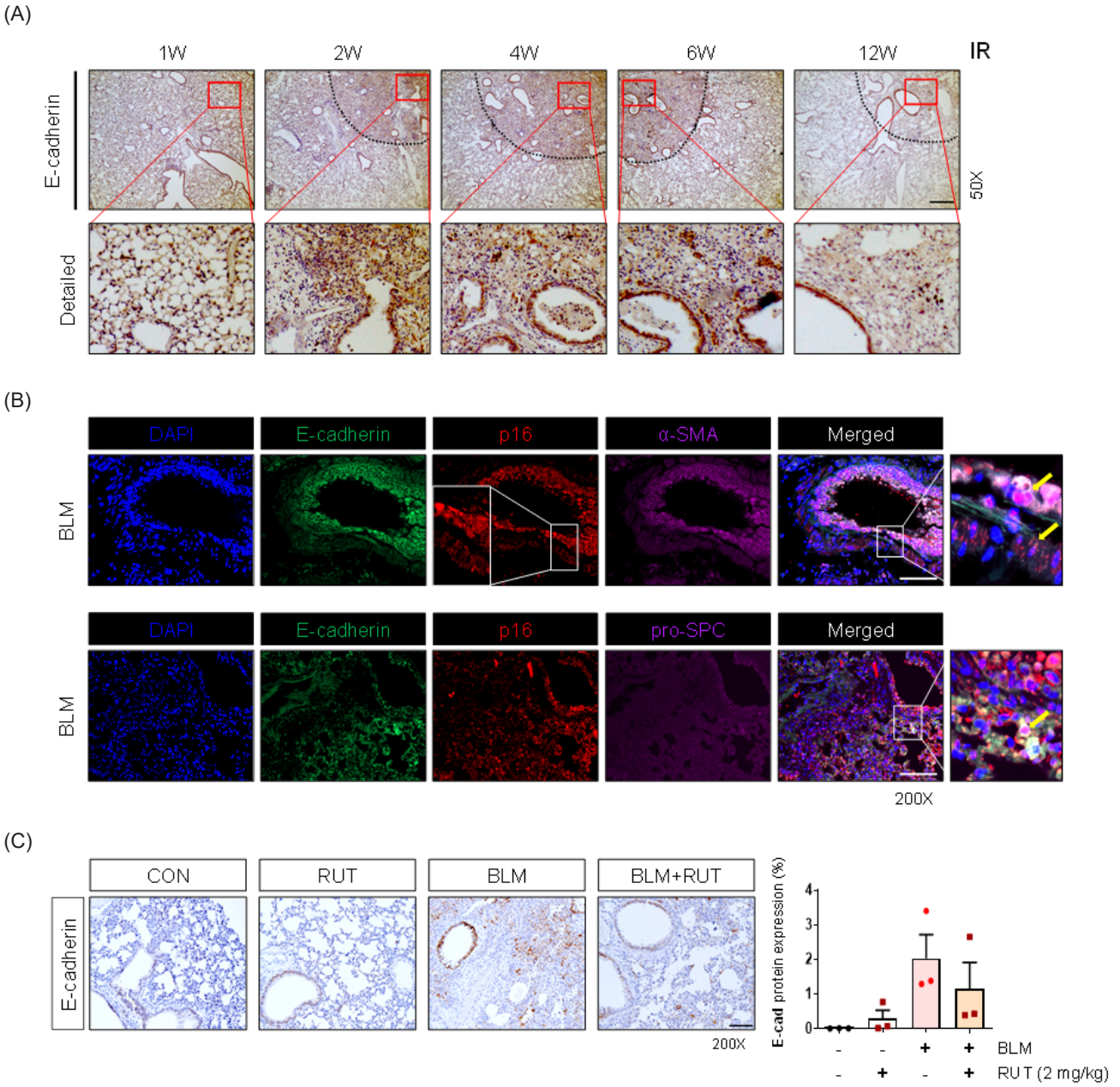

Fig. 3. Rutaecarpine attenuated E-cadherin expression in BLM-induced fibrosis model (A) Representative images of mouse lung sections stained with E-cadherin expression at indicated times after focal 75 Gy irradiation in IR-induced mouse PF model. Magnification, 50×. Scale bar, 100 μm. (B) Representative immunofluorescence image of E-cadherin (green), p16 (red), and α-SMA (violet) or pro-SPC (violet) in BLM-induced mouse PF model. Arrows indicate the p16-expressing cell types. Magnification, 200×. Scale bar, 100 μm. (C) Representative images of IHC analysis of E-cadherin positive areas in BLM-induced PF model. The graph shows the quantification of positive cells. Magnification, 200×. Scale bar, 100 μm.

epithelial cells are converted to mesenchymal cells. E-cadherin, a calcium-dependent adhesion molecule, is considered one of the key molecules involved in intercellular epithelial barrier formation. As a potential therapeutic target of fibrosis, a screening system to validate the activity of the promoter of E-cadherin was established. A natural compound library was screened and RUT, a bioactive alkaloid isolated from the fruit of *Evodia rutaecarpa*, was selected. Although RUT enhanced the activity of the promoter of E-cadherin, the underlying mechanism how RUT regulates E-cadherin promoter activity is unclear. RUT exerted anti-fibrotic effect through inhibiting TGF-β or BLM induced fibrotic features both *in vitro* and *in*

Table 1. The Primers sequence in qRT-PCR analysis.

Gene symbol	Forward primer	Reverse primer
Slug	CAACGCCTCCAAAAAGCCAA	ACTCACTCGCCCCAAAGATG
ZEB1	GGGGGAAAAGCGATCCTGAA	CTGTGTCATCCTCCCAGCAG
Snail	GCCTTTGTCCTGTAGCTCAAAGCA	CTTCTCACTGCCATGGAATTCCCT
Twist	GTCCGCAGTCTTACGAGGAGC	GCTTGAGGGTCTGAATCTTGCT
CDH1	AAAGGCCCATTTCCTAAAAACCT	TGCGTTCTCTATCCAGAGGCT

vivo models. These results may refer to the close relationship between pulmonary fibrosis and cellular senescence and RUT, an enhancer of E-cadherin, may contribute to a potential therapeutic strategy of targeting senescence in pulmonary fibrosis.

Acknowledgments

This research was funded by grants from the Basic Science Research Program (NRF-2022R1A2C200506113) and from the Basic Science Research Program (NRF-2017R1E1A1A01074674) through the National Research Foundation of Korea funded by the Ministry of Science, ICT and Planning. This work was supported by the Ewha Womans University Research Grant of 2024.

Conflicts of Interest Statement

The authors declare no competing interests.

References

(1) Maher, T. M.; Bendstrup, E.; Dron, L.; Langley, J.; Smith, G.; Khalid, J. M.; Patel, H.; Kreuter, M. *Respir. Res.* **2021**, *22*, 197.
(2) Schäfer, S. C.; Funke-Chambour, M.; Berezowska, S. *Pathologe* **2020**, *41*, 46–51.
(3) Glass, D. S.; Grossfeld, D.; Renna, H. A.; Agarwala, P.; Spiegler, P.; Kasselman, L. J.; Glass, A. D.; DeLeon, J.; Reiss, A. B. *Respir. Investig.* **2020**, *58*, 320–335.
(4) Liu, Y.-M.; Nepali, K.; Liou, J.-P. *J. Med. Chem.* **2017**, *60*, 527–553.
(5) Nieto, M. A.; Huang, R.Y.-J.; Jackson, R. A.; Thiery, J. P. *Cell* **2016**, *166*, 21–45.
(6) Thiery, J. P.; Acloque, H.; Huang, R. Y. J.; Nieto, M. A. *Cell* **2009**, *139*, 871–890.
(7) Williams, E. D.; Gao, D.; Redfern, A.; Thompson, E. W. *Nat. Rev. Cancer* **2019**, *19*, 716–732.
(8) Zavadil, J.; Böttinger, E. P. *Oncogene* **2005**, *24*, 5764–5774.
(9) Chanda, D.; Otoupalova, E.; Smith, S. R.; Volckaert, T.; De Langhe, S. P.; Thannickal, V. J. *Mol. Aspects Med.* **2019**, *65*, 56–69.
(10) Lin, Y.; Xu, Z. *Front. Cell Dev. Biol.* **2020**, *8*, 593283.
(11) Hohmann, M. S.; Habiel, D. M.; Coelho, A. L.; Verri Jr, W. A.; Hogaboam, C. M. *Am. J. Respir. Cell Mol. Biol.* **2019**, *60*, 28–40.
(12) Schafer, M. J.; White T. A.; Iijima K.; Haak, A. J.; Ligresti, G.; Atkinson, E. J.; Oberg, A. L.; Birch, J.; Salmonowicz, H.; Zhu, Y.; Mazula, D. L.; Brooks, R. W.; Fuhrmann-Stroissnigg, H.; Pirtskhalava, T.; Prakash, Y. S.; Tchkonia, T.; Robbins, P. D.; Aubry, M. C.; Passos, J. F.; Kirkland, J. L.; Tschumperlin, D. J.; Kita, H.; LeBrasseur, N. K. *Nat. Commun.* **2017**, *8*, 14532.
(13) Zhao, Y.; Zhou, X.; Zhao, Y.-L.; Gong, X.-J.; Zhao, C. *Molecules* **2015**, *20*, 2658–2667.
(14) Nguyen, N. V. T.; Lee, K. R.; Lee, Y. J.; Choi, S.; Kang, J. S.; Mar, W.; Kim, K. H. *J. Pharm. Biomed. Anal.* **2013**, *81-82*, 151–159.
(15) Tian, K.-M.; Li, J.-J.; Xu, S.-W. *Pharmacol. Res.* **2019**, *141*, 541–550.
(16) Gao, Y.-X.; Jiang, L.-L.; Zhang, Q.; Zuo, D.-Z.; Li, X.-W. *Zhongguo Zhong Yao Za Zhi* **2018**, *43*, 3530–3538.
(17) Zhang, H.; Zhu, K.; Zhang, X.; Ding, Y.; Zhu, B.; Meng, W.; Zhang, F. *Exp. Ther. Med.* **2022**, *23*, 373.
(18) Jin, H.; Jeon, S.; Kang, G.-Y.; Lee, H.-J.; Cho, J.; Lee, Y.-S. *Int. J. Radiat. Biol.* **2017**, *93*, 184–193.
(19) Kim, J.-Y.; Jeon, S.; Yoo, Y. J.; Jin, H.; Won, H. Y.; Yoon, K.; Hwang, E. S.; Lee, Y.-J.; Na, Y.; Cho, J.; Lee, Y.-S. *Clin. Cancer Res.* **2019**, *25*, 5364–5375.
(20) Habermann, A. C.; Gutierrez, A. J.; Bui, L. T.; Yahn, S. L.; Winters, N. I.; Calvi, C. L.; Peter, L.; Chung, M.-I.; Taylor, C. J.; Jetter, C.; Raju, L.; Roberson, J.; Ding, G.; Wood, L.; Sucre, J. M. S.; Richmond, B. W.; Serezani, A. P.; McDonnell, W. J.; Mallal, S. B.; Bacchetta, M. J.; Loyd, J. E.; Shaver, C. M.; Ware, L. B.; Bremner, R.; Walia, R.; Blackwell, T. S.; Banovich, N. E.; Kropski, J. A. *Sci. Adv.* **2020**, *6*, eaba1972

Received June 20, 2024
Revised August 14, 2024
Accepted August 26, 2024